Ferromagnetism in a dilute magnetic semiconductor: Generalized RKKY interaction and spin-wave excitations

Avinash Singh,[1,*] Animesh Datta,[2,†] Subrat K. Das,[1] and Vijay A. Singh[1]
[1]*Department of Physics, Indian Institute of Technology Kanpur - 208016, Kanpur, India*
[2]*Department of Electrical Engineering, Indian Institute of Technology Kanpur - 208016, Kanpur, India*
(Received 24 April 2003; revised manuscript received 30 July 2003; published 18 December 2003)

Carrier-mediated ferromagnetism in a dilute magnetic semiconductor has been studied using (i) a single-impurity based generalized Ruderman-Kittel-Kasuya-Yosida (RKKY) approach which goes beyond linear response theory, and (ii) a mean-field-plus-spin-fluctuation approach within a (purely fermionic) Hubbard-model representation of the magnetic impurities, which incorporates dynamical effects associated with finite frequency spin correlations in the ordered state. Due to a competition between the magnitude of the carrier spin polarization and its oscillation length scale, the ferromagnetic spin coupling is found to be optimized with respect to both hole doping concentration and impurity-carrier spin coupling energy J (or equivalently U). The ferromagnetic transition temperature T_c, deteremined within the spin-fluctuation theory, corresponds closely with the observed T_c values. Positional disorder of magnetic impurities causes significant stiffening of the high-energy spin-wave modes. We also explicitly study the stability/instability of the mean-field ferromagnetic state, which highlights the role of competing antiferromagnetic interactions causing spin twisting and noncollinear ferromagnetic ordering.

DOI: 10.1103/PhysRevB.68.235208 PACS number(s): 75.50.Pp, 75.30.Ds, 75.30.Gw

I. INTRODUCTION

The discovery of ferromagnetism in Mn-doped III-V semiconductors such as p-type $In_{1-x}Mn_xAs$, (Ref. 1) and $Ga_{1-x}Mn_xAs$,[2] with a highest transition temperature (T_c) of 110 K for a Mn concentration of $x=0.053$,[3] has led to considerable interest in these dilute magnetic semiconductors (DMSs). The successful search for ferromagnetic ordering above room temperature in $Ga_{1-x}Mn_xN$,[4,5] with a highest reported T_c value of 940 K,[6] has added a new dimension to the interest.

Besides their potential applications in semiconductor devices such as optical isolators, magnetic sensors, nonvolatile memories seamlessly integrated into semiconductor circuits, etc., and possibilities in photonics and high power electronics, attention has also been focused on the fundamental mechanism and nature of the ferromagnetic state, and the possibility of studying new magnetic cooperative phenomena such as spin-dependent tunneling, magnetoresistance, spin-dependent light emission, etc. in semiconductor heterostructures arising from the new (spin) degrees of freedom.

The double-exchange model, involving the interaction $-J\vec{S}_i.\vec{\sigma}_i$ between the magnetic impurity spin $\vec{S}_i$ and the electron spin $\vec{\sigma}_i$, has been the starting point in nearly all theoretical studies, and we first review the emerging physical picture and the different approaches employed.

Long-range ferromagnetic interaction between the $S=5/2$ Mn^{2+} ions is mediated, in the mean-field (Zener model) picture,[7–13] by a uniform itinerant-carrier spin polarization, which is caused, in turn, by an effective uniform magnetic field, resulting from a site averaging (virtual crystal approximation) of the local impurity fields. In the weak-field limit ($xJS \ll \epsilon_F$), the carrier spin polarization is proportional to the Pauli susceptibility χ_P, and the transition temperature ($T_c \sim xJ^2\chi_P$) is therefore proportional to the Mn concentration x, J^2, the carrier effective mass m^*, and $N(\epsilon_F) \sim p^{1/3}$, where p is the hole concentration. In DMSs, p is a only a small fraction (f) of x due to the large compensation by As antisite defects. Therefore, the Fermi energy $\epsilon_F \sim Wp^{2/3}$ itself is quite small compared to the bandwidth W, and hence the weak-field limit is valid only for $x \ll (W/JS)^3 f^2$. A valence band spin splitting comparable in size to the Fermi energy has been confirmed experimentally.[14]

Dynamical correlations in the ordered state have been studied within a path-integral formulation in which the itinerant carriers are integrated out and the effective action for the impurity spins is expanded up to quadratic order (noninteracting spin-wave approximation).[15] In contrast to the mean-field results, the spin stiffness (and hence T_c) is independent of J and inversely proportional to m. Other approaches incorporating dynamics include the dynamical mean-field theory,[16,17] in which the local charge and spin fluctuations are included but long-range spin-wave excitations are neglected, and a random phase approximation level spin-fluctuation approach in which Mn disorder is treated within the coherent potential approximation.[18]

While the positional disorder of Mn ions is not taken into account in the virtual crystal approximation (VCA), several recent works highlight the importance of disorder, both positional and electronic. The stability of the collinear ferromagnetic state has been investigated with randomly distributed Mn ions, and noncollinear ordering is suggested to be common to these semiconductor systems.[19] Competing (antiferromagnetic) interactions leading to frustration has already been evidenced by spin-glass behavior in II-VI DMSs.[20] The presence of large compensation due to As an-

tisite defects implies substantial electronic disorder as well, and the sensitivity of T_C, magnetization M, transport, and the spin-wave spectrum to disorder has been investigated.[21–25] Monte Carlo simulations have also been used to study disorder effects on magnetic ordering,[26–28] and dynamical and transport properties;[29] the background fermions determine the spin interactions and hence the nature of the spin ordering, which in turn affects the fermionic states. *Ab initio* methods[30–34] have also been recently employed.

An alternative mechanism for the ferromagnetic coupling between impurity spins involves the hole-mediated Ruderman-Kittel-Kasuya-Yosida (RKKY) interaction.[3] The RKKY theory has been extended for various dimensionality structures, including the effect of potential scattering through the carrier mean free path, indicating an enhancement of the ferromagnetic interaction by disorder in low dimensions.[7] Exchange and correlation has been shown to enhance T_C slightly within the RKKY theory.[9] Spin-wave dispersion in the RKKY picture has been compared with the result of spin-wave theory in which a uniform impurity-induced polarization has been assumed the (VCA), resulting in a Zeeman splitting Δ in the carrier bands.[15] It was shown that the RKKY-level dispersion is incorrect except when $\Delta \ll E_F$.

The traditional RKKY approach is based on linear response in the weak-field limit ($J \ll \epsilon_F$), which is not quite valid for the DMS. In this paper, we present a generalized RKKY approach which takes into account the spatial variation of the impurity-induced carrier spin polarization beyond linear response theory (Sec. II). In the generalized RKKY picture, the local magnetic field $\vec{B}_j = J\vec{S}_j$ of a magnetic impurity at site j polarizes the electrons locally, and the mobile band electrons spread this magnetic polarization in a characteristic manner: $\vec{m}_i = \chi_{ij}(B)\vec{B}_j$, where $\chi_{ij}(B)$ represents the generalized magnetic response. The spin $\vec{S}_i$ of another magnetic impurity placed at site i couples to this local electronic magnetization, resulting in an effective generalized RKKY spin coupling $J^2\chi_{ij}(J)\vec{S}_i \cdot \vec{S}_j$.

We find several interesting competing processes which limit the growth of spin couplings. As the RKKY response involves a particle-hole process, it vanishes for a filled (valence) band and grows with increasing hole concentration p. While the spin coupling is therefore expected to strengthen with p, a competing process involving the length scale sets in, which limits the growth of the spin coupling and therefore of the ferromagnetic transition temperature T_c. The Fermi wavelength $\lambda_F = 2\pi/k_F$, which sets the RKKY oscillation length scale, decreases with hole doping, and therefore the spin coupling between two magnetic impurities at a fixed separation goes through a maximum as a function of hole concentration (Sec. III).

We find a similar optimization in the spin coupling as a function of the impurity field strength B. By going beyond linear response theory, and examining the generalized RKKY response for a fixed hole concentration, we find that the RKKY oscillation becomes more rapid with increasing polarizing field. Therefore, for a fixed separation between two impurity spins, the spin coupling initially increases like J^2 as expected, but then crosses over and eventually changes sign, resulting in frustration (Sec. III). The nonlinear magnetic response thus brings out another limitation in the ferromagnetic spin coupling.

In order to determine the extent to which the magnetization response of a single impurity determines the macroscopic magnetic properties of the DMS, we have also considered a finite concentration of magnetic impurities distributed on a finite-size lattice (Sec. IV). Using a Hubbard-U representation for the magnetic impurities in a DMS, we have studied the collective magnetic response in the ferromagnetic state within a mean-field-plus-spin-fluctuation (MF+SF) approach. Treating the disorder aspects of the Mn-impurity system exactly, and electron correlation effects within the random phase approximation, our numerical analysis yields the spin stiffness from the low-lying collective (spin-wave) excitations (Sec. VI), which have a fundamental bearing on the ferromagnetic transition temperature T_c. Our approach also allows for a quantitative study of the stability/instability of the Hartree-Fock (mean-field) ferromagnetic state (Sec. V), highlighting the presence of competing interactions. The Anderson Hamiltonian, with a hybridization term V_{pd} between band fermions and the magnetic impurity orbital, has also been recently studied to obtain the ferromagnetic coupling between two magnetic impurities.[35]

II. MAGNETIC IMPURITY IN A HOST

We consider a single-band spin-fermion lattice model

$$H = \sum_{\mathbf{k},\sigma} \epsilon_{\mathbf{k}} a^{\dagger}_{\mathbf{k},\sigma} a_{\mathbf{k},\sigma} - \sum_i J_i \vec{S}_i \cdot \vec{\sigma}_i , \tag{1}$$

with a double-exchange interaction between the magnetic impurity spin $\vec{S}_i$ and the electron spin $\vec{\sigma}_i$ at the impurity site i. The host (valence band) dispersion $\epsilon_{\mathbf{k}}$ is taken to be parabolic for small k (top of the band at $k=0$), the k^2 coefficient determining the inverse carrier mass m^*. As the added holes go in long-wavelength states, the small-k particle-hole processes near the Fermi energy are dominant, and therefore other details of the energy band are expected to be relatively unimportant.

A. Host Green's function

We consider an isotropic energy-band dispersion

$$\epsilon_k = \frac{W}{2}\cos ka \tag{2}$$

in three dimensions, with the wave vector magnitude extending up to π/a. This dispersion incorporates the desired features, and yields a finite bandwidth without introducing sharp cutoffs. We choose length and energy units such that the lattice spacing $a=1$ and the bandwidth $W=1$. The advanced Green's function for the host is obtained as

$$g_{ij}(\omega) = \frac{1}{N}\sum_{\mathbf{k}} \frac{e^{i\mathbf{k}.(\mathbf{r}_i - \mathbf{r}_j)}}{\omega - \epsilon_{\mathbf{k}} - i\eta},$$

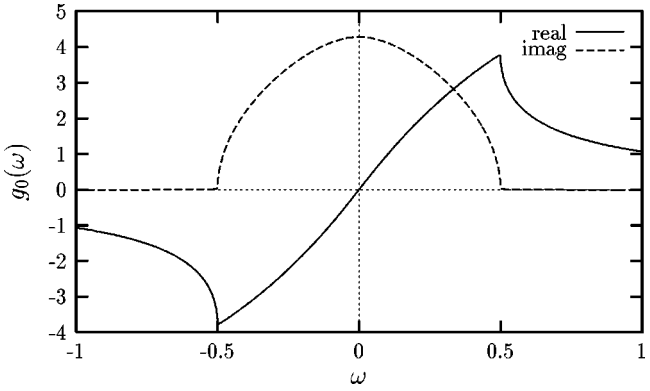

FIG. 1. Real and imaginary parts of the local host Green's function.

$$g_r(\omega)=\int_0^{\pi}\beta(k)dk\int_0^{\pi}\frac{1}{2}\sin\theta\ d\theta\frac{e^{ikr\cos\theta}}{\omega-\epsilon_k-i\eta}$$

$$=\int_0^{\pi}\beta(k)dk\frac{1}{\omega-\epsilon_k-i\eta}\frac{\sin kr}{kr}. \tag{3}$$

Here $\beta(k)$ is a k-space density of states, and for simplicity we choose a symmetric form

$$\beta(k)=ak^2-bk^4 \qquad (0\leqslant k\leqslant\pi/2)$$

$$=a(k-\pi)^2-b(k-\pi)^4 \qquad (\pi/2\leqslant k\leqslant\pi), \tag{4}$$

so that the usual three-dimensional k^2 form is recovered for states near both the lower and upper band edges at $k=\pi$ and $k=0$, respectively. We choose $b=2a/\pi^2$, so that $\beta(k)$ is smooth at $k=\pi/2$ (the slope $d\beta/dk=0$), and an overall normalization $a=120/7\pi^3$ so that the sum over states in the band $\int_0^{\pi}\beta(k)dk=1$.

The above choice yields a symmetric band with a nearly semielliptical density of states, as seen in Fig. 1, showing the real and imaginary parts of the local host Green's function $g_0(\omega)$. Near the band edges, the real-part magnitude has a finite maximum and the imaginary-part has a square-root behavior, as expected for the three-dimensional system. The band filling is shown in Fig. 2 as a function of the Fermi energy.

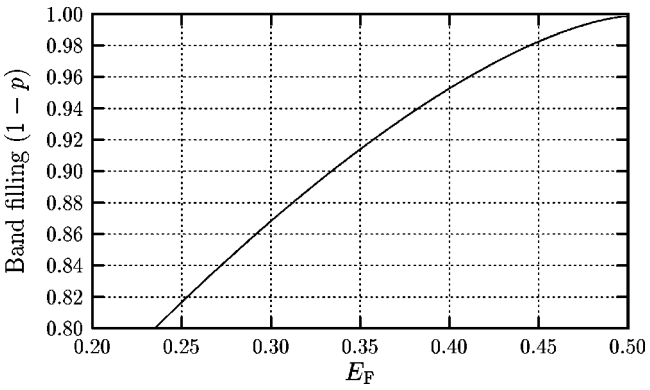

FIG. 2. Fermi energy dependence of the band filling.

B. Magnetic response

We consider the impurity spin in the classical limit ($J_i\vec{S}_i\rightarrow J_i\langle\vec{S}_i\rangle=B_i\hat{z}$), and examine the magnetic response of electrons in a nearly filled band due to the magnetic coupling $-\Sigma_i\vec{\sigma}_i\cdot\vec{B}_i$, for an arbitrary strength of the impurity-induced local magnetic field $\vec{B}_i$.

For a single magnetic impurity at site j, the electronic Green's function G is exactly obtained in terms of the host Green's function g as

$$G^{\sigma}_{ii}(\omega)=g_{ii}(\omega)+g_{ij}(\omega)\left[\frac{-\sigma B_j}{1+\sigma B_j g_0(\omega)}\right]g_{ji}(\omega), \tag{5}$$

where $g_0\equiv g_{jj}$ is the local host Green's function. The resulting local magnetization m_i at site i is then obtained as

$$m_i=\int_{-\infty}^{\omega_F}\frac{d\omega}{\pi}\mathrm{Im}[G^{\uparrow}_{ii}(\omega)-G^{\downarrow}_{ii}(\omega)], \tag{6}$$

where

$$G^{\uparrow}_{ii}(\omega)-G^{\downarrow}_{ii}(\omega)=g_{ij}(\omega)\ \Delta T_j g_{ji}(\omega), \tag{7}$$

in terms of the T-matrix difference

$$\Delta T_j\equiv T^{\uparrow}_j-T^{\downarrow}_j=\left[\frac{-2B_j}{1-B_j^2g_0^2(\omega)}\right]. \tag{8}$$

Defining a field-dependent generalized magnetic response function $\chi_{ij}(B)$ through the relation

$$m_i=\chi_{ij}(B)B_j, \tag{9}$$

Eqs. (6), (7), and (8) yield

$$\chi_{ij}(B)=\int_{-\infty}^{\omega_F}\frac{d\omega}{\pi}\mathrm{Im}\left[g_{ij}(\omega)\left(\frac{-2}{1-B^2g_0^2(\omega)}\right)g_{ji}(\omega)\right]. \tag{10}$$

III. EFFECTIVE SPIN COUPLINGS

Another impurity spin $\vec{S}_i$ placed at site i will couple with the local magnetization m_i produced by the local field of the spin $\vec{S}_j$ at site j, resulting in an effective interaction between the two spins given by

$$H_{\mathrm{spin}}(J)=-J_iJ_j\chi_{ij}(B=JS)\vec{S}_i\cdot\vec{S}_j. \tag{11}$$

A. Weak-coupling limit: RKKY interaction

When the B^2 term in Eq. (10) can be neglected (valid for $B\ll W$), one obtains a linear response

$$m_i=\chi_{ij}B_j, \tag{12}$$

where the magnetic susceptibility χ_{ij},

$$\chi_{ij}=-2\int_{-\infty}^{\infty}\frac{d\omega}{\pi}\ \mathrm{Im}[g_{ij}(\omega)g_{ji}(\omega)] \tag{13}$$

$$=4\sum_{\epsilon_l<\epsilon_F}\sum_{\epsilon_m>\epsilon_F}\frac{\phi^i_l\phi^{j*}_l\phi^j_m\phi^{i*}_m}{\epsilon_m-\epsilon_l},$$

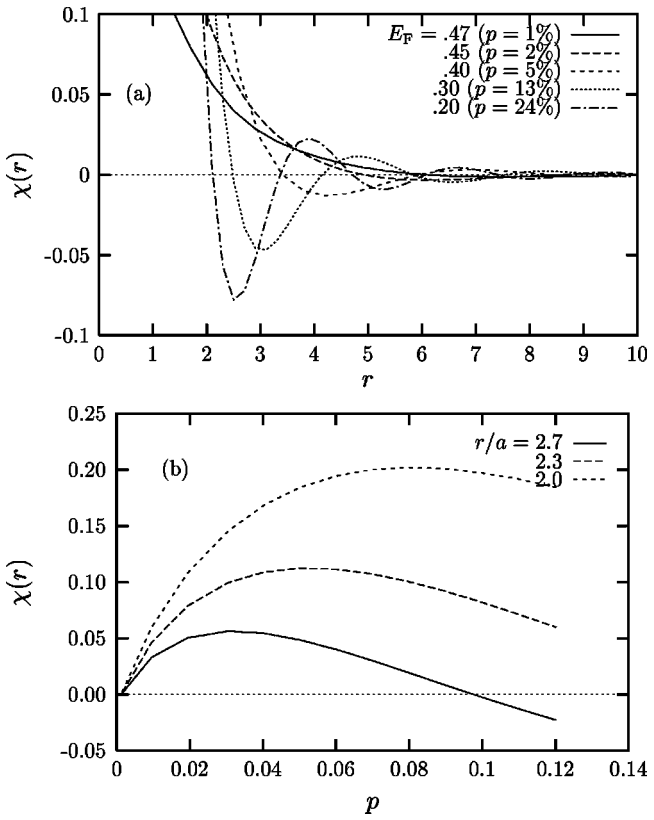

FIG. 3. The behavior of the magnetic susceptibility $\chi(r)$ (a) with r for different hole doping concentrations p, and (b) with p for different distances r (corresponding to average Mn-Mn separations in a cubic host lattice with 5%, 8%, and 12.5% Mn impurity concentration).

yields the standard oscillating RKKY interaction

$$H_{\mathrm{RKKY}} = -J_i J_j \chi_{ij} \vec{S}_i \cdot \vec{S}_j . \tag{14}$$

The behavior of χ_{ij}, as a function of the separation r betwen the two sites i and j, is shown in Fig. 3(a). The oscillation in $\chi(r)$ becomes more rapid with doping, as expected from the decreasing Fermi wavelength $\lambda_F = 2\pi/k_F$. Qualitatively similar results were obtained for a parabolic energy dispersion $\epsilon_{\mathbf{k}} \sim k^2$ with a finite bandwidth cutoff. For a fixed separation $r/a = (1/x)^{1/3}$, corresponding to the average Mn-Mn distance in a cubic lattice with Mn concentration x, the behavior of $\chi(r)$ is shown in Fig. 3(b) as a function of the hole concentration. The ferromagnetic coupling peaks at fractional hole concentration $p/x \approx 0.6$.

B. Generalized magnetic response

It appears that the conventional RKKY picture based on the weak-coupling limit ($B \ll W$) cannot provide a good description of the interaction between Mn impurities in $Ga_{1-x}Mn_xAs$. Core-level photoemission[36] yields $J \sim 1$ eV, which is comparable to the host bandwidth of $W \approx 2$ eV for the heavy hole band.[37] It is therefore essential to go beyond the linear-response regime, and for $B \sim W$ we find that there are additional contributions in the generalized magnetic response function $\chi_{ij}(B)$, which qualitatively modify the nature of the magnetic response and spin couplings.

1. Impurity-state contribution

For ω outside the band ($|\omega| > W/2$), the T-matrix difference in Eq. (10) has imaginary terms of the type $\delta(\omega - \omega^*)$, arising from the two poles

$$1 \pm B g_0(\omega^*) = 0, \tag{15}$$

corresponding to a spin-$\uparrow$ impurity state at $\omega^*_\uparrow$ (below the lower band edge), and a spin-$\downarrow$ impurity state at $\omega^*_\downarrow$ (above the upper band edge). In three dimensions, $g_0(\omega)$ has a finite maximum at the band edges, and therefore impurity states are formed only when B exceeds a threshold strength B^*.

By expanding $g_0(\omega)$ near $\omega^*_\uparrow$, and expressing $T^\uparrow_j$ as a simple pole, the impurity-induced correction is given by

$$G^\uparrow_{ii} - g_{ii} = g_{ij} T^\uparrow_j g_{ji} = \frac{|\varphi^\uparrow_i|^2}{\omega - \omega^*_\uparrow - i\eta}, \tag{16}$$

where the impurity-state wavefunction $\varphi^\uparrow_i$ is given by

$$\varphi^\uparrow_i = \frac{g_{ij}(\omega = \omega^*_\uparrow)}{\sqrt{-dg_0/d\omega|_{\omega=\omega^*_\uparrow}}}. \tag{17}$$

For any finite doping, only the spin-$\uparrow$ impurity state is occupied, and the impurity-state contribution to the local magnetization is therefore simply obtained as

$$m^*_i = |\varphi_i|^2. \tag{18}$$

With increasing B, the impurity-state wave function becomes more localized, and $\varphi_i \to \delta_{ij}$ as $B \to \infty$.

2. Band contribution

The other contributions to the imaginary part in Eq. (10) are from within the band ($|\omega| < W/2$), and involve the real (imaginary) part of $\Delta T_j(\omega)$ and the imaginary (real) part of $g_{ij}(\omega) g_{ji}(\omega)$.

Including both the band and impurity contributions, the generalized magnetic response $\chi(r,B)$ evaluated from Eq. (10) is shown in Fig. 4(a) for different field strengths; the lowest-field case ($B = 0.1$) provides the RKKY response ($B \to 0$), for comparison. The length scale at which the first crossover from ferromagnetic to antiferromagnetic coupling takes place is seen to decrease with increasing B. Figure 4(b) shows the magnetic field dependence of the generalized magnetic response $\chi(r,B)$, for a fixed hole concentration and Mn-Mn distance. For small $B = JS$, the response is essentially constant (linear response), and in this regime the generalized RKKY interaction energy $B^2\chi(r,B)$ grows like J^2, as in the mean-field and conventional RKKY pictures. However, the sharp suppression in the generalized magnetic response for $B/W > 0.2$ limits this growth and leads to a peak, which is seen to shift to higher B values with decreasing Mn-Mn separation (Fig. 5). This effect significantly increases the spin coupling in a higher Mn concentration sys-

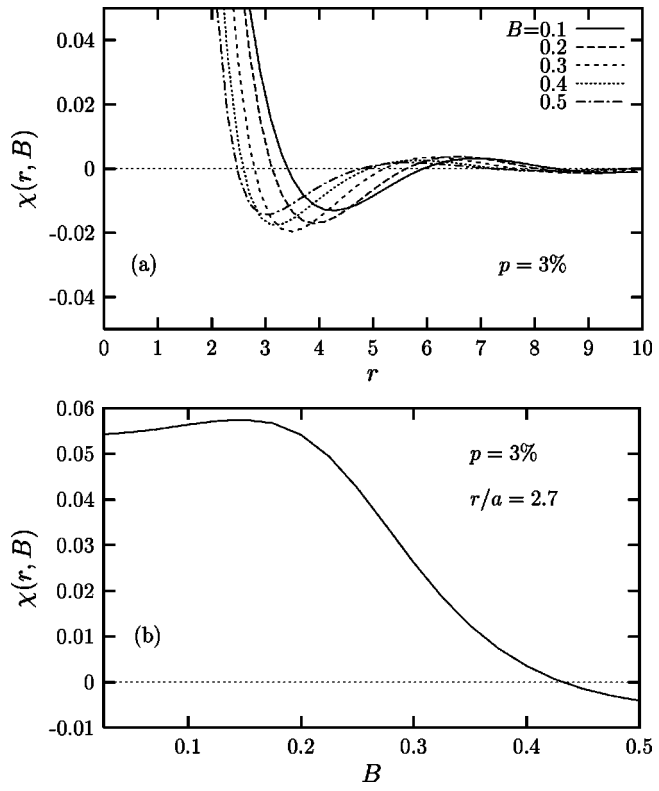

FIG. 4. The behavior of the generalized magnetic response $\chi(r,B)$ (a) with r for different field strengths B, and (b) with B for a fixed distance r. The hole concentration is fixed at $p=3\%$.

tem (such as GaMnN) beyond the factor expected from the spin response [Fig. 3(b)].

As the effective carrier mass m^* scales like the inverse bandwidth $1/W$, the m^* dependence of the generalized magnetic response $\chi(r,B)$ can be directly deduced from Fig. 4(b), showing the $B/W \propto m^*$ dependence for a fixed $B=JS$. The magnetic response in the (fixed) unit of $1/B$ is obtained by multiplying $\chi(r,B)$ in Fig. 4(b) (in unit of $1/W$) by B/W. This yields a linear m^* dependence of $\chi(r,B)$ (and hence the spin coupling energy and T_c) for a low effective mass and then a sharp suppression with increasing m^*. Sub-

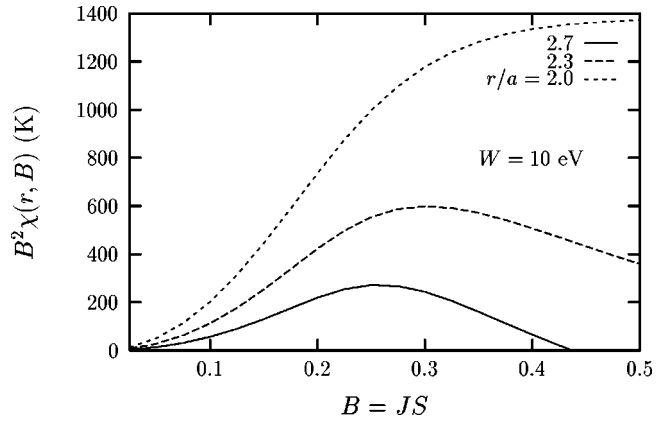

FIG. 5. The generalized RKKY interaction energy $B^2\chi(r,B)$ as a function of the local field strength B, for different Mn-Mn distances. The host bandwidth is nominally taken as 10 eV.

linear dependence of T_c at large m^* has also been reported in Monte Carlo studies.[26]

For a nominal host bandwidth of 10 eV (with 1 eV $\approx 10^4$ K), the peak interaction energies are about 250, 600, and 1400 K for Mn concentrations of 5%, 8%, and 12.5%, and hole concentrations of 3%, 5%, and 8%, respectively (Fig. 5). From this spin interaction energy $(JS)^2\chi$, the ferromagnetic transition temperature T_c can be estimated within the spin-fluctuation theory. For a nearest-neighbor quantum Heisenberg model (interaction energy $\mathcal{J}$) on a hypercubic lattice (coordination number z), the transition temperature is given by $T_c = T_c^{\rm MF}/f_{\rm sf}$, somewhat lower than the mean-field value $T_c^{\rm MF} = \mathcal{J}S(S+1)z/3$.[38] Here $f_{\rm sf} = (1/N)\Sigma_{\mathbf{k}}(1-\gamma_{\mathbf{k}})^{-1} \gtrsim 1$ is a geometrical spin-fluctuation factor, where $\gamma_{\mathbf{k}} \equiv (\cos k_x + \cos k_y + \cos k_z)/3$ in three dimensions.

As the effective RKKY interaction term between two spins is $J^2\chi_{ij}\vec{S}_i.\vec{S}_j$, we take $\mathcal{J}=J^2\chi$ and obtain $T_c \approx 2J^2\chi S(S+1)$ for $z=6$. Taking a realistic bandwidth of $W=2$ eV for the heavy valence band,[37] the peak energy in Fig. 5 translates to a peak T_c of about 150 and 850 K for 5% and 12.5% Mn concentrations, quite close to the observed highest T_c values for $Ga_{1-x}Mn_xAs$ and $Ga_{1-x}Mn_xN$.

IV. HUBBARD-*U* REPRESENTATION OF MAGNETIC IMPURITIES

We now consider a (purely fermionic) Hubbard-model representation for the randomly distributed magnetic impurities on a cubic lattice:

$$H = t\sum_{\langle ij\rangle\sigma}(\hat{a}^\dagger_{i\sigma}\hat{a}_{j\sigma} + \text{H.c.}) + t'\sum_{\langle Ij\rangle\sigma}(\hat{a}^\dagger_{I\sigma}\hat{a}_{j\sigma} + \text{H.c.}) + \epsilon_d\sum_{I,\sigma}\hat{a}^\dagger_{I\sigma}\hat{a}_{I\sigma} + U\sum_I(\hat{n}_{I\uparrow}-n_I)(\hat{n}_{I\downarrow}-n_I), \quad (19)$$

where I refers to the impurity sites, ϵ_d is the impurity on-site energy and $n_I = \langle \hat{n}_{I\uparrow} + \hat{n}_{I\downarrow}\rangle/2$ is the spin-averaged impurity charge density. Higher spin magnetic impurities, such as the $S=5/2$ Mn impurities in $Ga_{1-x}Mn_x$ As, can be realistically represented within a generalized Hubbard model representation involving multiple orbitals and different interaction processes (direct and exchange type, with respect to orbital indices).[39] For simplicity, we have taken the same hopping ($t'=t=1$) between the host-host and host-impurity nearest-neighbor pairs of sites. The energy-scale origin is set so that the host on-site energy is zero, and we take the impurity level to lie at the top of the host band ($\epsilon_d=6$). The form of the Hubbard interaction term is such that in the Hartree-Fock approximation it reduces to the double-exchange term.

A. Hartree-Fock ferromagnetic state

In the Hartree-Fock (mean-field) approximation, the interaction term reduces to a magnetic coupling of the electron to the local mean (magnetic) field $\vec{\Delta}_I$:

$$H_{\rm int}^{\rm HF} = -\sum_I \vec{\sigma}_I \cdot \vec{\Delta}_I, \quad (20)$$

where the electronic spin operator $\vec{\sigma}_I = \Psi_I^\dagger[\vec{\sigma}]\Psi_I$ in terms of the spinor $\Psi_I = \begin{pmatrix} \hat{a}_{I\uparrow} \\ \hat{a}_{I\downarrow} \end{pmatrix}$, and the mean field $\vec{\Delta}_I$, is self-consistently determined from the ground-state expectation value:

$$2\vec{\Delta}_I = U\langle\vec{\sigma}_I\rangle. \tag{21}$$

Thus, in the classical (Hartree-Fock) limit, the interaction term reduces to the corresponding form of the double-exchange term, with the mean field $\vec{\Delta}_I$ representing the impurity-induced local magnetic field $\vec{B}_I$.

Starting with an initial uniform mean field $\vec{\Delta}_I = \hat{z}\Delta$, the mean-field (MF) Hamiltonian is numerically diagonalized for a finite lattice to obtain the fermion eigenfunctions $\phi_{l\sigma}$ and eigenvalues $E_{l\sigma}$. The spin densities $n_{I\sigma} = \Sigma_{E_{l\sigma}<E_F}(\phi_{l\sigma}^I)^2$ yield the new local mean fields $\Delta_I = U(n_{I\uparrow} - n_{I\downarrow})/2$, which are then used to update the MF Hamiltonian, and this procedure is iterated until self-consistency is achieved.

B. Stability of the HF state

The self-consistent, HF ferromagnetic state, with all local moments aligned in the same symmetry-breaking direction, does not necessarily represent a stable (lowest-energy) state. This is because the HF state really represents an energy extremum, which may correspond to a saddle point having local energy minimum and maximum along different directions in the order-parameter space. The stability of the HF state with respect to transverse perturbations in the order parameter is indicated by the maximum eigenvalue $\lambda_{\max}$ of the $[\chi^0(\omega=0)]$ matrix [Eq. (24)].[40] The HF state is stable if $U\lambda_{\max}=1$, correspondng to the massless Goldstone mode, representing a rigid rotation of the ordering direction. Instability is indicated if $U\lambda_{\max}>1$, signaling a growth of transverse perturbations about the HF state, which can also be interpreted as negative-energy bosonic modes.

Figure 6(a) shows some of the eigenvalues of the $[\chi^0(\omega)]$ matrix (including the minimum and maximum) for the undoped HF ferromagnetic state of an 8^3 system, with a semi-ordered arrangement of 32 magnetic impurities (see Sec. V for details). For $\omega=0$, the Goldstone mode ($U\lambda_G=1$) is seen to correspond to the *lowest eigenvalue*, indicating maximal instability of the ferromagnetic state. The structure of the eigenvector corresponding to the maximum eigenvalue indicates a tendency towards antiferromagnetic (AF) ordering of the impurity spins. The AF coupling arises from the exchange interaction $J' \sim t'^2/U$ due to the effective hopping t' (associated with impurity-band formation) between impurity sites. In the absence of the hole-induced (RKKY) ferromagnetic coupling, this exchange interaction dominates and favors AF ordering of impurity spins. With hole doping, the ferromagnetic state is stabilized, and the Goldstone mode now corresponds to the maximum eigenvalue, as shown in Fig. 6(b).

For the impurity arrangements considered here, the self-consistency procedure rapidly converges to a (nearly) homogeneous ferromagnetic state of the DMS, even for finite doping, indicating its stability with respect to longitudinal fluctuations[41] in the local mean field Δ_I, inherent in the numerical process. However, for some impurity arrangements, the ferromagnetic state does exhibit mild longitudinal instability, leading to slow fluctuations in the impurity magnetization on few sites.[42]

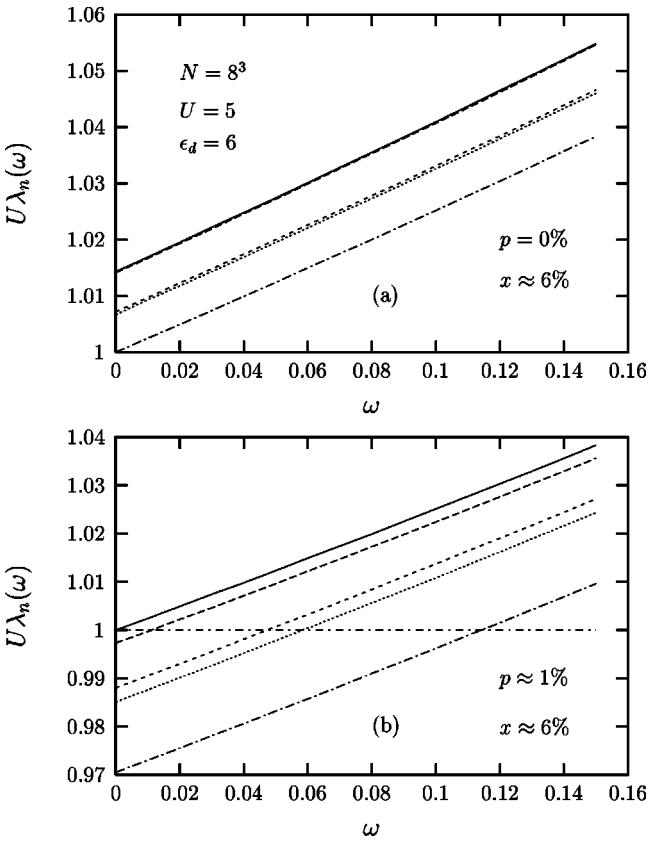

FIG. 6. (a) Instability of the undoped (HF) ferromagnetic state. The Goldstone mode ($U\lambda_G=1$) corresponds to the minimum eigenvalue of the $[\chi^0(\omega=0)]$ matrix, indicating maximal instability. (b) Stabilization of the ferromagnetic state with hole doping — the Goldstone mode now corresponds to the maximum eigenvalue.

C. Transverse spin fluctuations

Transverse spin fluctuations are gapless, low-energy excitations in the broken-symmetry state of magnetic systems possessing continuous spin-rotational symmetry. Therefore, at low temperatures they play an important role in diverse macroscopic properties such as existence of long-range order, magnitude and temperature dependence of the order parameter, magnetic transition temperatures, spin correlations, etc.

We study the time-ordered, spin-wave propagator involving the spin-lowering (S_i^-) and spin-raising (S_j^+) operators at sites i and j:

$$\chi_{ij}^{-+}(t-t') = i\langle\Psi_G|T[S_i^-(t)S_j^+(t')]|\Psi_G\rangle. \tag{22}$$

At the random phase approximately level, the spin-wave propagator in frequency space is given by

$$[\chi^{-+}(\omega)]=\frac{[\chi^0(\omega)]}{1-[U][\chi^0(\omega)]}, \tag{23}$$

where the zeroth-order, antiparallel-spin particle-hole propagator

$$\chi^0(\omega)]_{ij}=i\int\frac{d\omega'}{2\pi}G^{\uparrow}_{ij}(\omega')G^{\downarrow}_{ji}(\omega'-\omega)$$
$$=\sum_{E_l<E_F}^{E_m>E_F}\left(\frac{\phi^i_{l\uparrow}\phi^i_{m\downarrow}\phi^j_{m\downarrow}\phi^j_{l\uparrow}}{E_{m\downarrow}-E_{l\uparrow}+\omega}+\frac{\phi^i_{l\downarrow}\phi^i_{m\uparrow}\phi^j_{m\uparrow}\phi^j_{l\downarrow}}{E_{m\uparrow}-E_{l\downarrow}-\omega}\right) \tag{24}$$

is evaluated using the eigenvalues $E_{l\sigma}$ and eigenvectors $\phi_{l\sigma}$ in the self-consistent, broken-symmetry state. In Eq. (23), the diagonal interaction matrix $[U]_{ii}=U\delta_{iI}$ has nonvanishing elements only at the magnetic impurity sites. For site-dependent interactions, it is convenient to recast Eq. (23) using simple matrix manipulations:

$$[\chi^{-+}(\omega)]=\frac{1}{[A(\omega)]}-\frac{1}{[U]}, \tag{25}$$

where $[A(\omega)]=[U]-[U][\chi^0(\omega)][U]$ is a symmetric matrix, having nonvanishing matrix elements only in the reduced impurity basis:

$$[A(\omega)]_{IJ}=U(1-U[\chi^0(\omega)]_{IJ}). \tag{26}$$

Spin-wave modes, represented by the poles in the propagator $[\chi^{-+}(\omega)]$, are hence given by the poles of the matrix $[A(\omega)]_{IJ}$, as $[U]$ is nonsingular. In terms of the eigenvalues λ_n and eigenvectors φ_n of the $[\chi^0(\omega)]_{IJ}$ matrix, the spin-wave energies ω_n are therefore given by

$$1-U\lambda_n(\omega_n)=0. \tag{27}$$

V. SPIN-WAVE ENERGY

The spin couplings and stiffness in the ferromagnetic state can be determined from the spin-wave energies. To see how the magnitude and sign of the spin couplings depend on the impurity separation, we have considered several impurity arrangements with different numbers ($N_{\rm imp}$) of magnetic impurities in a cubic host lattice with $N=8^3$ sites. These arrangements include: (i) an ordered impurity arrangement of 64 impurities ($x=1/8$) on a cubic superlattice with impurity separation $2a$, (ii) a semiordered arrangement of 32 impurities ($x\approx 6\%$), with the same nearest neighbor (NN) impurity separation ($2a$) in the z direction but a greater in-plane separation ($\sqrt{8}a$), and (iii) a disordered arrangement of 30 impurities ($x\approx 6\%$) with NN separations ranging between $2a$ and $3a$.

For the undoped (insulating) state, we take $N_\uparrow=N$ and $N_\downarrow=N-N_{\rm imp}$; all spin-$\downarrow$ impurity states (pushed up by the local mean field) are then unoccupied, resulting in local-moment formation. Hole doping is introduced by reducing $N_\uparrow$, and band fillings are so chosen that the Fermi energy lies in gaps between (nearly) degenerate groups of eigenvalues.

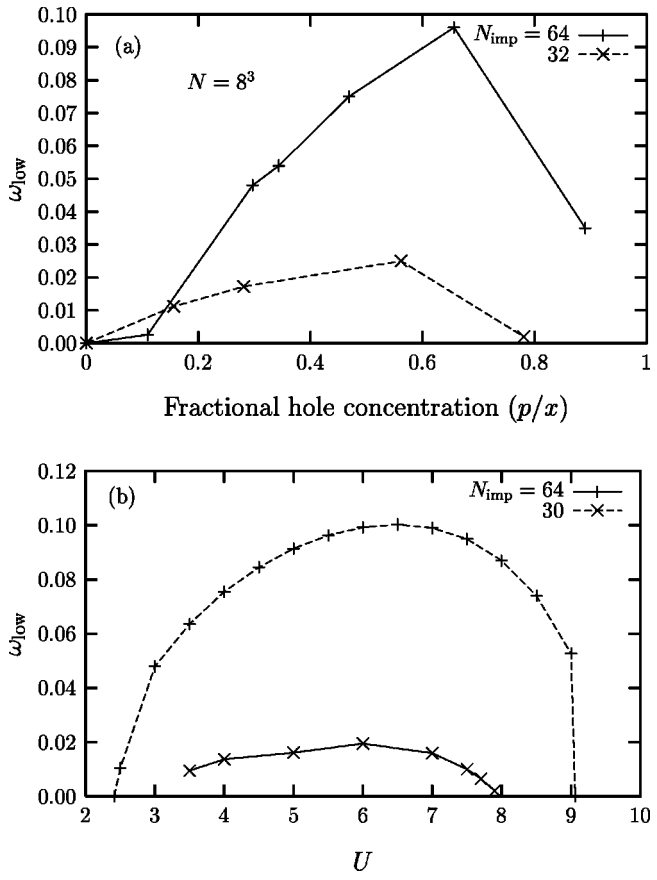

FIG. 7. Optimization of the lowest spin-wave energies for the ordered (+) and disordered (×) impurity arrangements (a) with fractional hole concentration (peak at $p/x\approx 0.6$) and (b) with U, similar to that of the RKKY ($J^2\chi$) and generalized RKKY spin couplings, shown in Figs. 3(b) and 5. An increasing impurity separation lowers the spin stiffness.

The undoped self-consistent ferromagnetic state is found to be maximally unstable, as discussed earlier. Indeed, the self-consistent antiferromagnetic state is actually found to be stable, confirming the dominance of the AF spin couplings $J'\sim t'^2/U$. With hole doping, the ferromagnetic state is stabilized, and the spin-wave energies ω_n are extracted from the pole condition $U\lambda_n(\omega_n)=1$. Hole doping and U dependences of the lowest spin-wave energy $\omega_{\rm low}$ are shown in Fig. 7 for the ordered and disordered impurity arrangements, with $U=4$ and 5, and $N_\uparrow=482$ ($p\approx 6\%$) and $N_\uparrow=505$ ($p\approx 1.4\%$), respectively. The optimization of the spin coupling with respect to both hole doping and interaction energy U is qualitatively similar to that in the RKKY picture.

While the lowest spin-wave energy is softened by disorder, the highest spin-wave energy is, however, significantly enhanced, as shown in Fig. 8. This enhancement of $\omega_{\rm high}$ is associated with localization of spin-wave states over impurity clusters in which the relatively closer spins are more

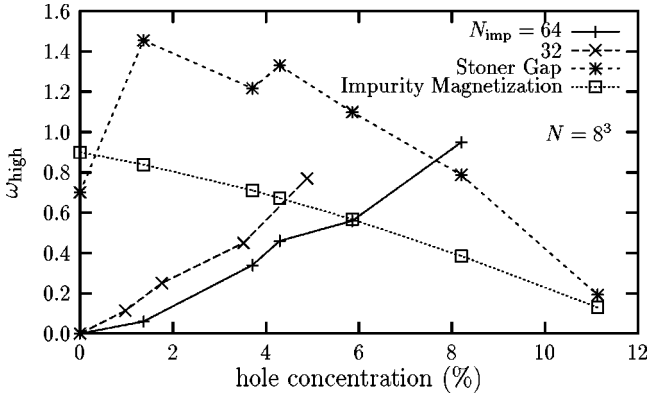

FIG. 8. The highest spin-wave energy for the ordered (+) and disordered (×) impurity arrangements, showing a disorder-induced stiffening of the high-energy mode.

strongly coupled.[42] For the *same* minimum impurity separation $(2a)$ in arrangements (i) and (ii), disorder-induced localization leads to stronger bonds between the cluster spins. Also shown (for the ordered case) is the Stoner (single-particle excitation) gap, which is roughly proportional to the MF impurity magnetization. The spin-wave branch merges with Stoner excitations at about 8% hole concentration.

For the ordered impurity arrangement, the spin-wave energy range allows the spin couplings to be extracted, as discussed below. Assuming a nearest-neighbor exchange interaction J between the impurity spins on the superlattice, the spin-wave energies are given by

$$\omega_{\mathbf{q}} = JSz(1-\gamma_{\mathbf{q}}), \tag{28}$$

where $\gamma_{\mathbf{q}} = (\cos q_x + \cos q_y + \cos q_z)/3$. The spin-wave modes on the impurity superlattice are plane waves, with wave-vector components given by $q_\mu = n_\mu 2\pi/L$, where n_μ are integers and $L=4$ for the 64-impurity superlattice. The wave vectors $\mathbf{q}=(1,0,0)2\pi/L$, etc. and $\mathbf{q}=(2,2,2)2\pi/L$ correspond to the lowest- and highest-energy modes, respectively. The corresponding energies $\omega_{\rm low} = JSz/3$ and $\omega_{\rm high} = 2JSz$ yield a ratio $\omega_{\rm high}/\omega_{\rm low} = 6$. We not only find the actual ratio to be quite close (≈ 7 for most doping cases), but the degeneracies in the spin-wave spectrum are also in close agreement, indicating that NN spin coupling is dominant.

VI. CONCLUSIONS

A comparitive study of a generalized RKKY approach and a MF+SF approach offers new and useful insight into the mechanism of carrier-mediated ferromagnetic ordering in a dilute magnetic semiconductor. While the MF+SF approach provides quantitative understanding of the spin couplings, competing interactions, spin-wave excitations, low-temperature spin dynamics, and the critical temperature, the generalized RKKY approach provides a qualitative understanding in terms of a simple physical picture involving the impurity-induced oscillating carrier-spin polarization, which complements the MF+SF approach. Our key finding is an optimization of the spin coupling (spin-wave energy) with respect to both hole doping and the impurity polarizing field strength (J or U), which is in agreement with a recent Monte Carlo study,[28] and can be physically understood in terms of a competition between the increasing magnitude of the carrier-spin polarization and the increasing rapidity of its oscillation. We find that the optimum (fractional) hole concentration for the spin coupling occurs at $p/x \approx 0.6$, and both the spin coupling energy $J^2\chi(r,J)$ and the spin-wave energy scale with the carrier bandwidth W, for fixed J/W or U/W. The oscillating spin polarization also highlights the role of competing interactions in the instability of the collinear ferromagnetic state.

In this paper, we have presented a study of spin-wave excitations in the ferromagnetic state of a DMS within a microscopic correlated lattice fermion model which treats finite impurity concentration, impurity disorder, and electron correlation on an equal footing. With regard to electron correlation, the MF+SF approach has been extensively used in the context of strongly correlated layered cuprate antiferromagnets which exhibit pronounced spin fluctuations.[43] When the spin-wave energy is much smaller than the mean-field strength Δ, spin dynamics is dominant at low temperatures and charge fluctuations can be ignored for $T \ll \Delta$. Incorporating the low-energy spin fluctuations about the MF state yields a quantitatively correct temperature dependence of (sublattice) magnetization and reliable $T_{\rm C}$ within the renormalized spin-wave theory.[43] Whereas $T_{\rm C}$ pertains to global ordering, with the spin coupling energy providing the relevant energy scale for spin fluctuations, the mean-field theory deals with local ordering, and greatly overestimates the transition temperature ($T_{\rm C} \sim \Delta$), which really represents the moment-melting temperature.

Specifically with regard to the DMS, there is a subtle issue concerning the energy scale relevant for global ordering. Whereas for a generic ferromagnet, energy scales corresponding to the local mean field and spin coupling are identical, for the DMS, three distinct energies can be identified — the two local mean fields seen by the carrier spin ($\sim J$) and impurity spin ($\sim J^2\chi_{ii}$), and the coupling between impurity spins ($\sim J^2\chi_{ij}$). In the weak doping limit ($p/x \to 0$), the magnetic response function $\chi(r)$ decays slowly on the impurity-separation scale, so that $\chi_{ij} \approx \chi_{ii}$, and the distinction between the two latter energy scales becomes blurred. However, for a realistic fractional doping of $p/x \approx 15\%$, the impurity spin coupling $J^2\chi_{ij}$ is by far the lowest energy scale, and should therefore control the low-temperature behavior of the magnetization $M(T)$. The ferromagnetic transition temperature T_c, determined within the spin-wave-theory from the spin-coupling energy for a realistic (heavy) hole bandwidth, corresponds closely to the observed T_c values in $Ga_{1-x}Mn_xAs$ and $Ga_{1-x}Mn_xN$. With appropriate hole doping, a transition temperature much above room temperature appears possible for $x = 1/8$, which is within experimental limit.[44]

The MF+SF approach also highlights the role of impurity disorder. While the low-energy spin-wave modes are significantly softened as compared to the ordered case, the high-energy spin-wave modes are clearly stiffened, indicating that a single spin-wave energy scale is not sufficient to describe the low-temperature spin dynamics in the DMS. In fact, a

distribution in spin couplings, with weak and strong bonds, has been suggested to be responsible for the anomalous temperature dependence of the magnetization, susceptibility, specific heat, etc.[45] Using a simple model involving two spin-excitation energy scales corresponding to weakly and strongly coupled spins, the temperature dependence of magnetization is found to be in good agreement with the superconducting quantum interference device magnetization data for $Ga_{1-x}Mn_xAs$.[42]

ACKNOWLEDGMENTS

Helpful discussions with T. Pareek and R. C. Budhani are gratefully acknowledged.

*Electronic address: avinas@iitk.ac.in

†Present address: Department of Physics and Astronomy, University of New Mexico, Albuquerque, New Mexico 87131, USA.

[1] H. Ohno, H. Munekata, T. Penny, S. von Molnar, and L. L. Chang, Phys. Rev. Lett. **68**, 2664 (1992).

[2] H. Ohno, A. Shen, F. Matsukara, A. Oiwa, A. Endo, S. Katsumoto, and Y. Iye, Appl. Phys. Lett. **69**, 363 (1996).

[3] F. Matsukara, H. Ohno, A. Shen, and Y. Sugawara, Phys. Rev. B **57**, R2037 (1998).

[4] N. Theodoropolpu *et al.*, Appl. Phys. Lett. **78**, 3475 (2001).

[5] M. L. Reed *et al.*, Appl. Phys. Lett. **79**, 3473 (2001).

[6] S. Sonoda *et al.*, J. Cryst. Growth **237–239**, 1358 (2002).

[7] T. Dietl, A. Haury, and Y. M. d'Aubigne, Phys. Rev. B **55**, R3347 (1997).

[8] M. Takahashi, Phys. Rev. B **56**, 7389 (1997).

[9] T. Jungworth, W. A. Atkinson, B. H. Lee, and A. H. MacDonald, Phys. Rev. B **59**, 9818 (1999); B. H. Lee, T. Jungworth, and A. H. MacDonald, *ibid.* **61**, 15 606 (2000).

[10] T. Dietl, H. Ohno, F. Matsukara, J. Cibert, and D. Ferrand, Science **287**, 1019 (2000).

[11] T. Dietl, H. Ohno, and F. Matsukara, cond-mat/007190 (unpublished).

[12] T. Dietl, F. Matsukara, and H. Ohno, Phys. Rev. B **66**, 033203 (2002).

[13] T. Jungworth, J. König, J. Sinova, K. Kučera, and A. H. MacDonald, Phys. Rev. B **66**, 012402 (2002).

[14] H. Ohno, N. Akiba, F. Matsukara, A. Shen, K. Ohtani, and Y. Ohno, Appl. Phys. Lett. **73**, 363 (1998).

[15] J. König, H. H. Lin, and A. H. MacDonald, Phys. Rev. Lett. **84**, 5628 (2000); J. König, T. Jungworth, and A. H. MacDonald, Phys. Rev. B **64**, 184423 (2001).

[16] A. Chattopadhyay, S. Das Sarma, and A. J. Millis, Phys. Rev. Lett. **87**, 227202 (2001).

[17] S. Das Sarma, E. H. Hwang, and A. Kaminski, cond-mat/0211496 (unpublished).

[18] G. Bouzerar and T. P. Pareek, Phys. Rev. B **65**, 153203 (2002).

[19] J. Schliemann and A. H. MacDonald, Phys. Rev. Lett. **88**, 137201 (2002).

[20] J. K. Furdyna and J. Kossut, *Diluted Magnetic Semiconductors*, Semiconductors and Semimetals Vol. 25 (Academic Press, New York, 1988).

[21] M. Berciu and R. N. Bhatt, Phys. Rev. Lett. **87**, 107203 (2001).

[22] A. L. Chudnovskiy and D. Pfannkuche, Phys. Rev. B **65**, 165216 (2002).

[23] M. Berciu and R. N. Bhatt, Phys. Rev. B **66**, 085207 (2002).

[24] G. Bouzerar, J. Kudrnovský, and P. Bruno, cond-mat/0208596 (unpublished).

[25] C. Timm, F. Schäfer, and F. von Oppen, Phys. Rev. Lett. **89**, 137201 (2002); C. Timm and F. von Oppen, J. Supercond. **16**, 23 (2003); cond-mat/0209055 (unpublished).

[26] J. Schliemann, J. König, and A. H. MacDonald, Phys. Rev. B **64**, 165201 (2001).

[27] M. P. Kennett, M. Berciu, and R. N. Bhatt, Phys. Rev. B **66**, 045207 (2002).

[28] G. Alvarez, M. Mayr, and E. Dagotto, Phys. Rev. Lett. **89**, 277202 (2002).

[29] G. Alvarez and E. Dagotto, Phys. Rev. B **68**, 045202 (2003).

[30] H. Akai, Phys. Rev. Lett. **81**, 3002 (1998).

[31] M. Shirai *et al.*, J. Magn. Magn. Mater. **177–181**, 1383 (1998).

[32] S. Sanvito, P. Ordejón, and N. A. Hill, Phys. Rev. B **63**, 165206 (2001).

[33] L. M. Sandratskii and P. Bruno, Phys. Rev. B **66**, 134435 (2002).

[34] L. Craco, M. S. Laad, and E. Müller-Hartmann, cond-mat/030342 (unpublished).

[35] V. A. Ivanov, P. M. Krstajić, F. M. Peeters, V. Fleurov, and K. Kikoin, Europhys. Lett. **61**, 235 (2003).

[36] J. Okabayashi *et al.*, Phys. Rev. B **58**, R4211 (1998).

[37] J. R. Chelikowski and M. L. Cohen, Phys. Rev. B **14**, 556 (1976); W. A. Harrison, *Electronic Structure and the Properties of Solids* (Freeman, San Francisco, 1980).

[38] M. E. Lines, Phys. Rev. **135**, A1336 (1964); S. Doniach and E. H. Sondheimer, *Green's Functions for Solid State Physicists* (Benjamin, New York, 1974).

[39] A. Singh and P. Sen, Phys. Rev. B **57**, 10 598 (1998).

[40] For a stability analysis of the hole and electron doped antiferromagnetic state, see A. Singh and Z. Tešanović, Phys. Rev. B **41**, 614 (1990); A. Singh and H. Ghosh, *ibid.* **65**, 134414 (2002).

[41] In contrast, the AF state of the Hubbard model (with nearest neighor hopping) is unstable to longitudinal fluctuations upon hole doping, leading to formation of spin bags[J. R. Schrieffer, X.-G. Wen, and S.-C. Zhang, Phys. Rev. Lett. **60**, 944 (1988)] and stripes[D. Poilblanc and T. M. Rice, Phys. Rev. B **39**, 9749 (1989).] It is the degeneracy at the nested Fermi surface which significantly enhances the susceptibility to longitudinal fluctuations, as evidenced by the stabilization of the homogeneous antiferromagnetic state when this degeneracy is lifted, e.g., by a small next-nearest-neighbour hopping term (Ref. 40).

[42] A. Singh, cond-mat/0307009 (unpublished).

[43] A. Singh, cond-mat/9802047 (unpublished); Eur. Phys. J. B **11**, 5 (1999), and references therein.

[44] A. J. Blattner and B. W. Wessels, cond-mat/0205602 (unpublished).

[45] M. P. Kennett, M. Berciu, and R. N. Bhatt, Phys. Rev. B **65**, 115308 (2002).